Investigation on pool-scrubbing hydrodynamics with VOF interface-capturing method

Liao, Y.; Li, J.; Lucas, D.;

Originally published:

March 2022

Nuclear Engineering and Design 390(2022), 111713

DOI: https://doi.org/10.1016/j.nucengdes.2022.111713

Perma-Link to Publication Repository of HZDR:

https://www.hzdr.de/publications/Publ-33305

Highlights

Investigation on pool-scrubbing hydrodynamics with VOF interface-capturing method

Yixiang Liao,Jiadong Li,Dirk Lucas

- Hydrodynamic phenomena in pool scrubbing analyzed in detail with the VOF method.
- Both time-averaged phase distribution and instantaneous bubble properties well captured.
- Significant globule breakup at high flow rates observed in the injection region.
- Coalescence and short residence time at high flow rates may affect particle retention.
- Effect of liquid recirculation and gas entrainment at the free surface needs further analysis.

Investigation on pool-scrubbing hydrodynamics with VOF interface-capturing method

Yixiang Liao[a,*], Jiadong Li[b,a] and Dirk Lucas[a]

[a]Helmholtz-Zentrum Dresden-Rossendorf, Institute of Fluid dynamics, Bautzner Landstraße 400, 01328 Dresden, Germany
[b]School of Energy Science and Engineering, Central South University, 410083 Changsha, China

ARTICLE INFO

Keywords:
Aerosol particle
Decontamination factor
OpenFOAM
Pool scrubbing
VOF interface-capturing

ABSTRACT

Pool scrubbing with bubble swarm generated by gas jet is an effective technique for aerosol retention at severe accidents, owing to large interfacial area and long residence time. Correct understanding of the process and thus enhancing its efficiency relies on analysis of the hydrodynamic behaviour of the gas, since it affects particle removal mechanisms directly. The objective of the present work is to explore the gas jet structure in detail by means of VOF interface-capturing method and additional techniques for tracking bubble characteristics and trajectories. The main findings are: a) The breakup of globules in the injection zone becomes significant at high gas flow rates and has a great contribution in particle removal; b) The increase of bubble size and velocity with the injection velocity will promote the inertial and centrifugal deposition of aerosol particles; c) However, the coalescence probability of rising bubbles is found to increase with the gas flow rate, which may influence particle retention by re-enclosing particles from liquid film and reducing surface area; d) Furthermore, the reduction in bubble residence time as they rise through the pool is unfavourable for particle removal. Nevertheless, liquid recirculation originated from violent interaction between the gas jet and the pool surface as well as swarm effects helps to prolong the residence of bubbles. The effect of gas flow rates on the decontamination factor is found to be associated with a variety of gas-liquid hydrodynamic phenomena. The proposed numerical approach is capable of acquiring detailed local information that is required for model development. Both the time-averaged spatial distribution of void fraction and the instantaneous size/rise velocity of individual bubbles obtained from the simulation conform to the experimental data. In the next step it will be extended to include aerosol particles.

1. Introduction

Release of aerosols and radionuclides frequently occurs as a result of severe accidents of nuclear power plants, e.g. steam generator tube rupture or hot core debris interacting with pressure vessel concrete. The radioactive particles make their way to the containment atmosphere or the secondary side bypassing the primary barrier, which has been a topic of intensive research in the nuclear safety analysis. Analyzing the release, transport and retention of aerosol and fission products reliably is essential for quantifying the amount of radioactivity that ultimately reaches the environment. In water-cooled power plants such as PWR (pressurized water reactor) and BWR (boiling water reactor), large water pools are often present in the transport passage of the aerosols, and contribute to attenuate the magnitude of ultimate release, which is referred to as pool scrubbing. For instance, in BWR's, the fission product- or aerosol-laden steam-gas mixture is directed to the suppression pool where steam is condensed to avoid over-pressurization of the wet well space, while in PWR's, the aerosol mixture could pass through the pressurizer quench tanks before reaching the containment, or leak to the secondary-side pool of a steam generator following a heat transfer tube rupture. Furthermore, many nuclear power plants worldwide have installed filtered containment venting systems (FCVSs), where the wet scrubber is a key component. Therefore, from the safety analysis point of view it is of significance to study aerosol bubble rising throught water pools and determine particle retention rate. The efficiency of aerosol trapping is usually represented in terms of the decontamination factor (DF), which is defined as the fraction of particles that are retained in the pool proportional to the amount that is injected totally. It is a focus of most important studies including both experimental and numerical. In the PASSAM project (Albiol et al., 2017) pool scrubbing was addressed as a first priority topic, and related activities constitute the biggest work-package. Most experiments put effort into the decontamination factor as well as the influence of some design parameters such as the nozzle submergence, particle size and gas injection rate.

*Corresponding author
y.liao@hzdr.de (Y. Liao)

For example, the ACE experiments in EPRI reported that the pool depth positively influenced the retention efficiency of aerosol particles (Berzal et al., 1995). According to the LACE experiment carried out at CIEMAT (Marcos et al., 1994) the particle removal efficiency decreases with their size. The PSEIDON-II experiments of PSI showed that DF increases with the gas injection flow rate (Dehbi et al., 2001). Li et al. (2021) suggested that the DF increases exponentially with the pool depth. In low-depth pool scrubbing the mechanism of steam condensation was found be dominant while the effect of particle diameter is negligible. The experiments performed at the PECA facility (Peyres et al., 1995) revealed that there existed an additional removal mechanism independent of submergence. It is supposed to be related to the hydrodynamic behaviour of high-speed gas jets at the injection. The role of the injection nozzle size was stressed by Kim et al. (2021) considering that it influences some key parameters like gas velocity and globule diameter at the nozzle. In their experiment the DF was found to decrease from 197 to 6.2 as the nozzle diameter increased from 5 mm to 30 mm. RSE (Morandi et al., 2015) pointed out one significant weakness in the existing experiments that tracking of influencing parameters like bubble size and shape was lacking, and carried out an experimental campaign on hydrodynamics with injection velocities from 16 to 74 m/s. The results revealed that local void fraction and bubble size distributions were similar in the swarm rise zone, while the hydrodynamic condition in the injection zone depends on the injection velocity and water composition. The presence of surfactants or electrolytes influences the probability of coalescence and breakup, leading to smaller globule sizes and higher retention efficiencies (Abe et al., 2018). More recent studies dedicated to acquiring CFD-level data on phase distribution and bubble dynamics, which is essentially useful for the validation of CFD simulation results. Abe et al. (2018) and Nakamura et al. (2019) conducted experiments on the flow structure of gas-phase jet into a water pool, and obtained the bubble size, aspect ratio, rising velocity and local void fraction by means of wire-mesh sensors (WMS). Yoon and Jeong (2019) studied the flow behavior evolving from bubbly to jet regime with a high-speed camera, and measured void fraction and bubble velocity using the dual-sensor optical fiber method. Fujiwara et al. (2019) carried on visualization experiments on the internal flow and aerosol movement inside a silicone oil droplet simulating an air bubble.

Multiple hydrodynamic phenomena taking place during the pool scrubbing were found contributing to the retention efficiency of aerosol particles. The flow regime can be classified roughly with reference to the Weber number (We) criterion, which is defined on the basis of gas injection velocity and nozzle diameter (Ma et al., 2019; Yoon and Jeong, 2019). In the globule ($10^3 < We < 10^5$) and jet ($We > 10^5$) regime, the scrubbing region can be divided into three zones: injection, breakup and rise. Each zone is associated with certain phenomena that scrub aerosols in the pool. In the injection zone, particles are not able to follow the gas trajectory and are deemed to be removed majorly through inertial collision with the bubble surface apart from the condensation of steam. The collapse of large globules in the breakup zone has also a significant contribution to the scrubbing efficiency, while in the swarm rise region, the removal efficiency is influenced largely by the motion of bubble and particle. In overall, the mechanisms comprise centrifugal force and impaction with the interface, gravitational sedimentation, Brownian diffusion and vapor evaporation/condensation. Hydrodynamic variables characterizing these processes such as particle sedimentation velocity, bubble shape, size and rising velocity are required for the determination of the DF, often missing in the experiments. In a lumped parameter code, these parameters are usually evaluated by the rule of thumb or extrapolation outside the range of validity of some empirical correlations. The uncertainty increases with the jet flow rate. On the other hand, the capability of CFD for multi-phase flows is improved rapidly in the past decades, and the methodology is accepted as an integral part of product design and safety analysis in many industries, among which is nuclear power industry (Khan et al., 2021, 2020; Wang et al., 2021). It is able to provide insights into the hydrodynamic phenomena that take place in the pool scrubbing, informing about local hydrodynamic variables and help to reduce the uncertainty in estimating the DF and subsequent radioactivity release. Hence, CFD investigation on bubble dynamics in pool scrubbing is included in one work package of the IPRESCA project (Gupta et al., 2017) to quantify modelling uncertainties, evaluate existing models in system codes e.g. ASTEC, COCOSYS, MELCOR (Marchetto and Cousin, 2019). In the frame of this project, CFD benchmark cases are defined, and pure water-air systems are considered in the first two steps (Dehbi et al., 2022). The results reported in this paper are part of these benchmark cases, which explore the pool-scrubbing hydrodynamics by using the VOF (volume of fluid) interface-capturing methodology in OpenFOAM. In a water-air-aerosol system the retention of aerosols is majorly credited to their interaction with the air-water interface, which is dependent on various motion mechanisms as discussed above. In the reality, radioactive fission products carrying large amount of heat result in heat and mass transfer as well as chemical reaction in the pool, which affect the decontamination factor. Furthermore, the carrier gas of aerosols usually comprises a mixture of steam and non-condensable gases, and steam-aerosol scrubbing is substantially different from air-aerosol scrubbing, since interfacial mass transfer alters the bubble size and dynamics like coalescence and breakup greatly (Liao and Lucas, 2016). In addition, steam

condensation is significant in the injection zone, which has been found to be a dominant mechanism for low-depth scrubbing in the experiment of Li et al. (2021). On the other hand, Fujiwara et al. (2019) showed that the motion and dynamics of bubbles was affected by the presence of aerosol particles as well their solubility. The complicity of these phenomena as well as their effects on the decontamination factor will be studied step by step in the future research.

After introducing the general framework of the VOF methodology and interFOAM solver in Section 2, a brief summary of the investigated test cases and numerical setups is given in Section 3. The main results from the simulations and their comparison with the experimental data are presented in detail in Section 4. Finally, a short discussion on the overall performance of the numerical method and future perspectives in Section 5 concludes the paper.

2. Numerical method

Pool scrubbing like hydrodynamic breakup, atomization of diesel jet and air entrainment by a plunging jet is characterized with extensive topology changes. For successfully simulating this type of flow situations the implicit interface capturing methods like VOF and level-set have attracted significant attention, among which interFOAM as an open-source VOF methodology has been receiving increased amount of usage (Deshpande et al., 2012; Maiwald and Schwarze, 2011; Srinivasan et al., 2011). The solver is designed for two Newtonian, incompressible, isothermal, and immiscible fluids, which means that the material properties are constant in the region filled with one of the fluids except at the interface, and one set of equations are solved for the whole domain. The continuity and momentum equations are expressed as follows.

$$\frac{\partial U_j}{\partial x_j} = 0 \tag{1}$$

$$\frac{\partial \rho U_i}{\partial t} + \frac{\partial \rho U_j U_i}{\partial x_j} = -\frac{\partial p}{\partial x_i} + \frac{\partial}{\partial x_j}\left(\mu\left(\frac{\partial U_i}{\partial x_j} + \frac{\partial U_j}{\partial x_i}\right)\right) + \rho g_i + f_{\sigma i} \tag{2}$$

with

$$\rho = \rho_g \alpha + \rho_l (1-\alpha) \tag{3}$$

$$\mu = \mu_g \alpha + \mu_l (1-\alpha) \tag{4}$$

where ρ_g, ρ_l and μ_g, μ_l are the density and viscosity of gas and liquid, which are set as constant according to the experimental conditions. α representing the void fraction, is 1 inside gas and 0 inside liquid, while at the interface varies between 0 and 1. In order to "identify" or "capture" the interface an additonal equation for α has to be solved.

$$\frac{\partial \alpha}{\partial t} + \frac{\partial \alpha U_j}{\partial x_j} = 0 \tag{5}$$

The MULES algorthim is used to ensure that α remains between 0 and 1. For the sharpening of interface the standard interface compression scheme with vanLeer interpolation in interFOAM (Weller, 2006) is adopted. The surface tension force in Eq. 2, $f_{\sigma i}$, is modelled as a volumetric force using the continuum surface force (CSF) method proposed by Brackbill et al. (1992). The methodology has been successfully utitlized to analyze bubble formation, growth and detachment from submerged orifices in many works, e.g. Albadawi et al. (2013); Boubendir et al. (2020); Georgoulas et al. (2015). Preliminary results for pool-scrubbing conditions have been reported by Okagaki et al. (2020) and Liao and Lucas (2020) recently. In the simulation, no turbulence models are activated to the gas and liquid phases by assuming that the small-scale velocity fluctuations are adequately resolved by the computational mesh. The assumption is reasonable for stagnant liquid pool with low gas void fractions ($\alpha < 0.5\%$). Nevertheless, it would be interesting to investigate the effect of turbulence models in the future study in particular at presence of aerosols.

3. Investigated cases and numerical settings

The VOF methodology presented above is applied in simulating the experiments of Abe et al. (2018), who investigated the flow structure of gas jet in pool scrubbing and obtained the bubble size, aspect ratio void fraction and bubble velocity distribution by using wire-mesh sensors in addition to high-speed video cameras. The work is selected considering that data sets important for the validation of numerical results are available, which are in contrast missing in most other pool-scrubbing experiments. The experimental pool has a square cross section of width $b = 500\ mm$. The circular nozzle for gas injection has an inner diameter of 6 mm, and its submergence is 1100 mm, see Figure 1 (a). The material system was air-water, and experiments were carried out at room temperature and atmospheric pressure. Accordingly, the material properties of $\rho_l = 1000\ kg{\cdot}m^{-3}$, $\mu_l = 10^{-3}\ Pa{\cdot}s$, $\rho_g = 1\ kg{\cdot}m^{-3}$, $\mu_g = 1.48{\times}10^{-5}\ Pa{\cdot}s$ are specified for the liquid and gas phase in the numerical study, respectively, and the surface tension coefficient is assumed 0.07 N/m. Two-layer wire mesh sensors were mounted at five height positions, i.e. $z = 100,\ 300,\ 500,\ 700,\ 900\ mm$, z representing vertical distance from the nozzle exit. The distribution of void fraction and gas velocity as well as equivalent spherical diameter of bubbles were measured by the wire-mesh sensor, whose interference on the flow field was not discussed yet. In addition, bubble size, aspect ratio and rise velocity can be obtained by processing the high-speed images. For further details about the measurement and data acquisition the reader are referred to the original work of Abe et al. (2018).

Four gas flow rates, $\dot{Q} = 8.5,\ 42.4,\ 84.8,\ 254.0\ l/min$, were measured, and the first three cases are investigated numerically in the present work. They correspond to an injection velocity of $U_{inj} = 5.0,\ 25.0,\ 50.0,\ 150.0\ m/s$, and the Weber number is in the order of $10^3, 10^4, 10^5, 10^6$, respectively. The computational domain is close to the real geometry but with some minor simplifications. As shown in Figure 1 (a) the nozzle is represented with a hole in the bottom plate, and the submerged part is neglected. This simplification has been made frequently in the numerical study on bubble injection such as in Quan and Hua (2008) and Georgoulas et al. (2015). In addition, to keep the computational cost acceptable, the pool height is restrained to the nozzle submergence, which is the distance between the free surface and the nozzle exit, equal to 1100 mm in the experiment. The effect of air cushion above the free surface was investigated separately, which was found to have a negligible effect on the distribution of average hydrodynamic parameters such as void fraction and velocity, but some difference in the instantaneous snapshots of void fraction is observable, which should be looked at more closely in the future study on aerosol scrubbing. The mesh has a uniform resolution of 1 mm in the vertical direction while the cross section is locally refined at the centre, where the nozzle is located, see Figures 1 (b) and (c). The lateral length of peripheral cells is 5 mm, where most of time only single-phase liquid is present. The refined region have cells of a size varying from 0.4 to 1.0 mm, and is connected with the surroundings through a transition region. The total number of cells exceeds 10^7. The computational cost for the three cases is evaluated at the end.

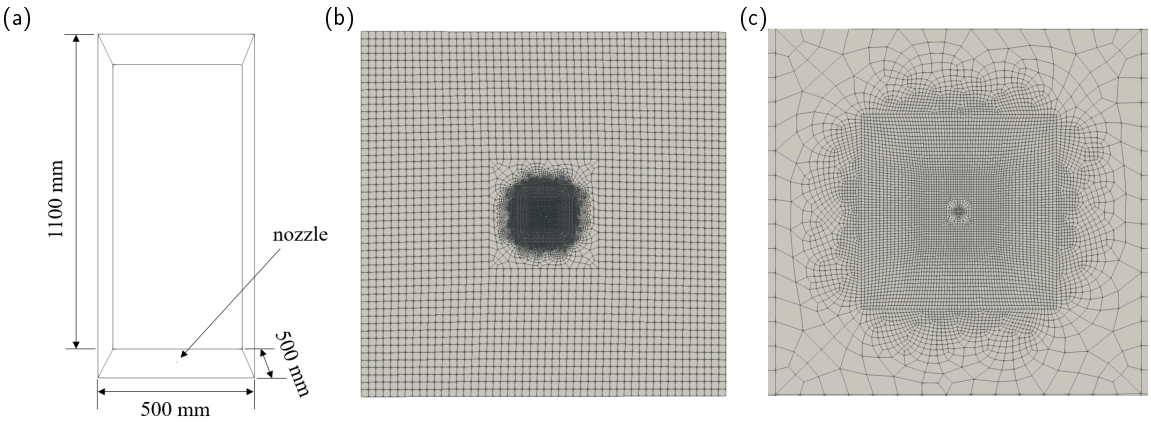

Figure 1: Sketch of computational domain, geometry and mesh size

As aforementioned the simulations in the present study are performed with the OpenFOAM v8.0 software, and the VOF solver interFOAM is adopted, which is able to describe the gas-jet disintegration and bubble-swarm structure. For the solution of Eqs. 1 ∼ 5 following boundary conditions are applied for the three unknowns α, p and U_j, see Table

1, where p_{rgh} is related to p in this way

$$p_{rgh} = p - \rho g \left(h - h_{ref}\right) \tag{6}$$

with h_{ref} as the reference height. The *zeroGradient* boundary condition, as the name suggests, simply extrapolates the quantity from the nearest cell to the boundary, e.g. the wall. The void fraction is assumed to have the *inletOutlet* condition at the outlet boundary, which works like *zeroGradient* when the fluid flows outside of the domain and like a $fixedValue$ one when the flow enters the domain. In this study only air is allowed to flow reversely through the outlet. The injection of pure air through the nozzle is realized by fixing $\alpha = 1$ at the inlet. No-slip condition at the wall is applied for the velocity. The inlet value is determined according to the experimental conditions of volumetric flow rates and nozzle cross-section area. The $pressureInletOutletVelocity$ boundary condition for the velocity assigns a *zeroGradient* condition for flow out of the domain, but for inflow the normal velocity is allowed to find its own value, which is set to zero in this work. The static pressure at the outlet is specified to 0 Pa with the boundary condition $prghPressure$, while the pressure gradient at the inlet and wall is set by $fixedFluxPressure$ such that the fluxes on these boundaries conform to the velocity boundary condition. Since there is no fluxes through the wall, it is equivalent to a *zeroGradient* condition there.

Variable	Wall	Outlet	Inlet (nozzle)
α	zeroGradient	inletOutlet	fixedValue
U_j	no-slip	pressureInletOutletVelocity	fixedValue
p_{rgh}	fixedFluxPressure	prghPressure	fixedFluxPressure

Table 1: Summary of boundary conditions applied in the simulation

To control the computational speed appropriately an adjustable time step was introduced with an initial value of 10^{-5} in conjunction with a limit for the Courant number (Co). In the VOF algorithm it is important to keep the Courant number at the interface to be small enough, which is determined by local mesh size and velocity. In the present work, it is set to be 0.5, while the Courant number for the mean flow is limited to 2.0. As a result the actual time step for the three investigated cases is in the order of 10^{-5}, which decreases with the increase of gas injection flow rate. More details will be provided by the end of the next section. Standard interpolation schemes for interFOAM are used with $GausslimitedLinearV$ 1 for the velocity component advection term and *Gauss linear* for the stress term. The velocity-pressure coupling is solved using the PIMPLE (merged PISO-SIMPLE) algorithm, thereby, the limit of $Co < 1$ is overcome and the simulation can be speeded up. The number of outer correction loops is set to 2, which means that the pressure-momentum coupling is calculated twice in one time step. Total 20 seconds physical time of the injection process are simulated in each case, over which time-averaged results are calculated.

4. Numerical results

The gas-jet structure is visualized with snapshots of 3D void fraction contours ($\alpha = 0.5$) in Figure 2, where in each case the left picture is from experiment and the right one from simulation. At low gas flow rates ($We < 10^2$), a gas injected into stagnant liquid pool will form bubbles, which grow and detach from the nozzle periodically and non-interferingly. The departure size is nearly constant, depending on the balance between various forces that the bubble is subjected to such as gravity, inertial, buoyancy and surface tension. This is called bubbling regime (Barron et al., 2020). As the gas flow rate increases, the interaction between successively detached bubbles becomes significant. The bubble adjourns above the nozzle after departing. Its wake influences the period and size of subsequent bubbles departing, and coalesces with them or absorb a part of them eventually, which results in non-uniform departure of bubbles concerning size and frequency (Zhang and Shoji, 2001). The position of coalescence becomes closer to the nozzle with the increase of injection velocity, leading to large globules at departure or even continuous gas structures connected with the nozzle exit. This is called globule or jetting regime, and the transition occurs at $We = 10^5$ according to the work of Yoon and Jeong (2019). As seen from Figure 2 the cases in the present study all belong to the jetting regime or bubbling to jetting transition, which is typical in pool scrubbing scenarios under acccidental conditions but requires further study in particular with interface-capturing methods. Both the experiment and simulation snapshot images show that in the cases of $\dot{Q} = 8.5\ l/min$ and $\dot{Q} = 42.4\ l/min$ the globule rises away from the nozzle after coalescence between two

successive bubbles, and the size of globules increases with the gas flow rate. At $\dot{Q} = 84.8\ l/min$ the coalesced bubble does not detach from the nozzle immediately, merging with a third bubble and forms a continuous gas, because its injection Weber number reaches 2×10^5. The feature of void structure in the injection region is qualitatively well reflected by the numerical model.

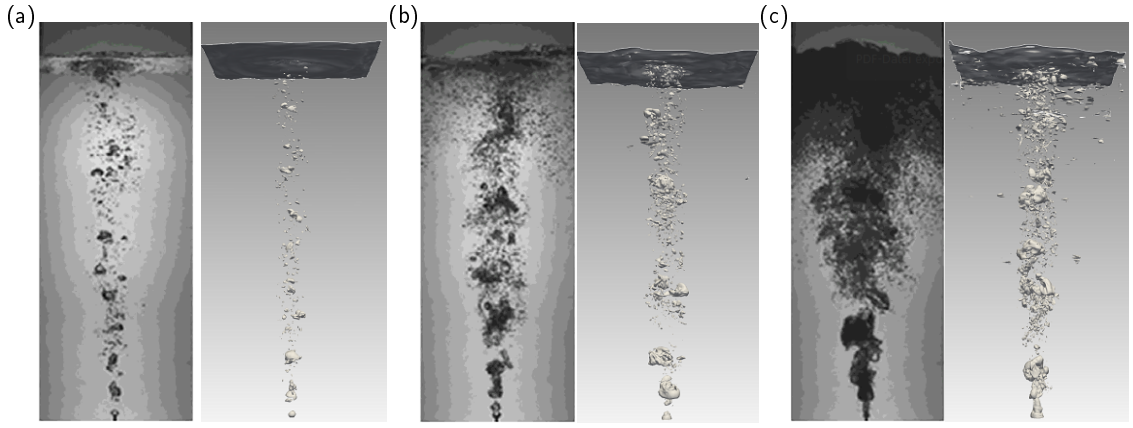

Figure 2: Snapshots of the void fraction contours at $t = 20\ s$ ((a) $\dot{Q} = 8.5$ l/min, (b) $\dot{Q} = 42.4$ l/min, (c) $\dot{Q} = 84.8$ l/min, left: experiment, right: simulation)

The formation and evolution of gas-jet structure near the injection nozzle is presented in further detail in Figure 3. The globules are elongated remarkably in the axial direction of the nozzle (from left to right), and interact with each other violently. After departure the large globule has a pear-like shape with a pointed top due to the rapid growth of next bubble taking place at the nozzle. The globule base remains unclosed, and a low-pressure region is formed inside the detached bubble. The subsequent one is absorbed into it shortly after its appearance, e.g. at $t = 0.0875$ s. The rest gas at the nozzle exit is stretched into a cylindrical shape and detaches earlier than its predecessor. The rising globule pinches off as the horizontal size of its base exceeds a certain value and the internal pressure drops below some value, and a bubble ring is formed behind. The next detached bubble goes through the ring, reaching the main part of the bubble and interacts with it further. There are no isolated bubbles observed near the orifice during the formation of bubbles in all the three cases. The departure size and frequency of globules increases with the gas flow rate, and becomes aperiodic under these conditions. As pointed out by Peyres et al. (1995), it is quite difficult to correlate the data for globule diameter at an injection flow higher than 60 l/min. In addition to steam condensation, the

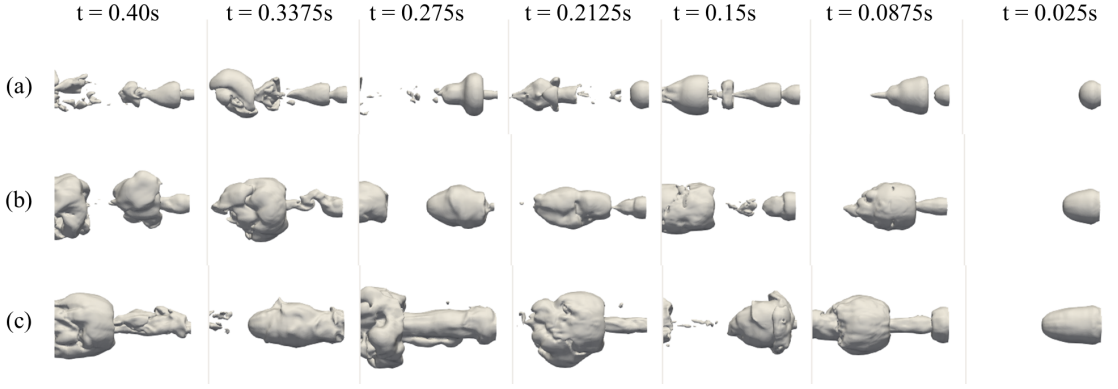

Figure 3: Formation and disintegration of gas jet near the injection nozzle ((a) $\dot{Q} = 8.5$ l/min, (b) $\dot{Q} = 42.4$ l/min, (c) $\dot{Q} = 84.8$ l/min)

disintegration of globules is an important mechanism responsible for particle removal in the injection region, which

demands more effort both experimentally and numerically. As the tests using the RSE SCRUPOS facility showed, the injection velocity and water composition have a clear impact on the bubble size distribution in the injection zone, and consequently the scrubbing efficiency (Albiol et al., 2018). In the range far away from the nozzle exit, which is called rise region, a bubble swarm is formed as the result of coalescence and breakup, while the number and size of bubbles increase as the gas flow rate increases. At the low injection velocity the bubble plume characteristics, e.g. width and number concentration, obtained from the experiment and simulation are in a qualitatively good agreement. As the velocity increases, the interaction between rising bubbles and the free surface becomes more intensive, which leads to a large number of small bubbles forming beneath the free surface. They travel downwards through the liquid pool along with the recirculation, and the penetration deepth increases with the gas injection velocity, as the experimental high-speed video images in Figure 2 (b) and (c) show. The formation of these bubbles results from gas entrainment by drop impacts. Violent interaction between the bubble swarm and free surface generates splashing droplets. Some of them will be entrained by the scrubbed gas flow and becomes a secondary pollution source, which has been studied in many works of nuclear safety analyses (Ouallal et al., 2021). On the other hand, the droplets may collect particles from the gas via inertial impaction, interception or other mechanisms (Berna et al., 2016). Nevertheless, most of the droplets will fall back and impact on the liquid surface, which may entrain bubbles into the pool as observed in this work. There are a variety of mechanisms govern this entrainment process (Hale and Akers, 2016; Pumphrey and Elmore, 1990; Tran et al., 2013), which however cannot be described by the present model appropriately. For such purpose further extensions of the outlet boundary condition are necessary, although the entering of gas into the pool through the free surface is allowed in current studies. Compared to droplet entrainment occuring above the pool surface, the phenomenon of gas entrainment has received less attention. However, it influences the pool hydrodynamics evidently, and the effect on aerosol scrubbing efficiency needs further investigation.

Since bubble size is a key parameter determining the decontamination factor, the OpenFOAM function object regionSizeDistribution is applied to provide insights about the instantaneous size distribution of bubbles inside the pool. At $t = 20s$, in total 365, 1040 and 1685 bubbles are detected in the cases of $\dot{Q} = 8.5\ l/min, 42.4\ l/min$ and $84.8\ l/min$, respectively. The minimum size is around 1.2 mm while the maximum value exceeds 30 mm, as shown in Figure 4. In consistence with the experimental observation (Abe et al., 2018; Peyres et al., 1995), a log-normal like function is capable of fitting the data satisfactorily, and the mean lies close to $d = 4.25\ mm$. The gas flow rate seems to have little impact on the distribution shape and the Sauter mean diameter, which varies from 4.2 mm in case (a) to 4.7 mm case (c). The explanation is that most of the bubbles are detected in the swarm rise region, where the gas flow rate has little influence on bubble size distribution as proved by the recent RSE experiments (Morandi et al., 2015).

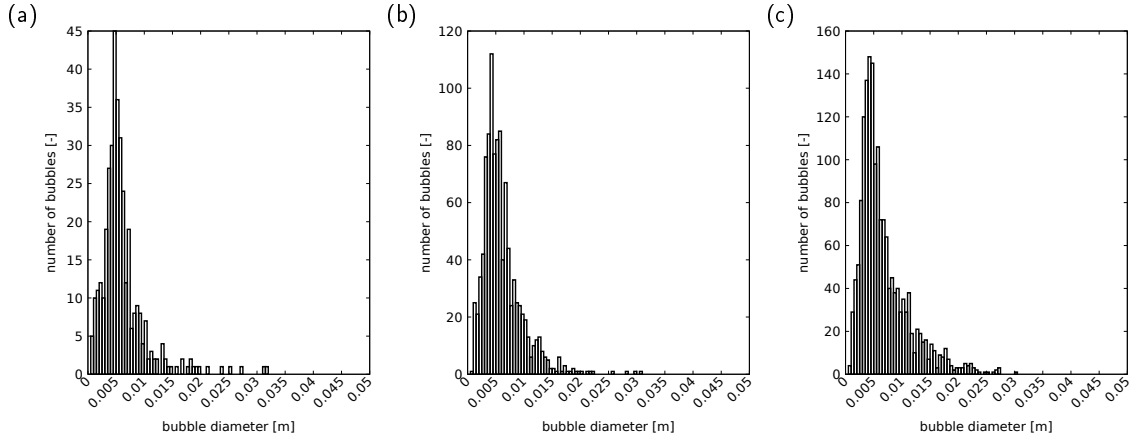

Figure 4: Bubble size distribution in the whole domain evaluated at t=20 s ((a) $\dot{Q} = 8.5$ l/min, (b) $\dot{Q} = 42.4$ l/min, (c) $\dot{Q} = 84.8$ l/min)

In the simulation all bubbles are tracked over the whole lifetime by means of additional tracking techniques. The evolution and distribution of bubble size along the way from nozzle exit towards free surface is illustrated in Figure 5, which reveals the influence of injection rates on bubble dynamics. In the case of $\dot{Q} = 8.5\ l/min$, the size of globules at detachment is around 23 mm, and noticeable coalescence takes place thereafter, which increases the size over 30 mm.

At a distance of about 200 *mm* above the nozzle exit the bubble size decreases minorly due to breakup, which conforms to the experimental observations of Abe et al. (2018) and Albiol et al. (2018). While in the rise region ($z = 0.3 \sim 0.8\ m$) the size of bubbles remains nearly unchanged, a slight reduction is observed close to the free surface. As the gas flow rate increases, the detached globule size increases obviously, reaching 43 *mm* at $\dot{Q} = 84.8\ l/min$. Because of high interfacial stress and surface instability violent breakup or disintegration events instead of coalescence are observed in the injection region, while in the rise zone large bubbles are formed as a result of coalescence. At high gas injection rates the maximum bubble size increases continuously up to the free surface. At the same time, the number of small and medium bubbles increases. The dynamic processes of bubble coalescence and breakup that take place simultaneously in pool scrubbing are proven to have a considerable impact on the particle retention efficiency. In general, the breakup of aerosol bubbles contribute to removing particles while coalescence between bubbles may re-enclose particles from the liquid. As pointed out by Peyres et al. (1995) the primary breakup occuring at high injection velocities is expected to contribute to the pool retention significantly, which is even able to compensate the effect of submergence. From the numerical point of view coalescence and breakup is still a complex challenging topic in particular with the two-fluid approach. In three-phase systems, the model assumptions should take into account particle effects in addition to bubble approaching velocities. As Fujiwara et al. (2019) showed the bubble shape and rising velocity were affected by the aerosol inside it; soluble aerosols had a similar effect as surfactants. On the other hand, particles inside the liquid are known to have a significant influence on the bubble coalescence and breakup. A classical theory is that they tend to increase the effective slurry viscosity (Kadoi and Nakae, 2011), which changes the bubble wake, vortex shedding, bubble deformation and collision frequency and so on. Apart from uncertainties contained in initial globule diameters, as they rise through liquid pool or column, a variety of interaction with the liquid as well as among themselves may disintegrate them or drive them to coalesce, e.g. buoyancy and wake. The superimposition of various mechanisms increases the modelling difficulty drastically (Liao et al., 2014; Risso and Fabre, 1998). Separate effect tests by means of experiment or simulation would be necessary to fully validate the mechansims. Further studies on the effect of gas flow rates and accompanying hydrodynamics as well as particle effects on the bubble size distribution are desirable for the determination of DF, apart from that of inlet gas composition, nozzle size, submergence as well as pool temperature, which has been extensively investigated.

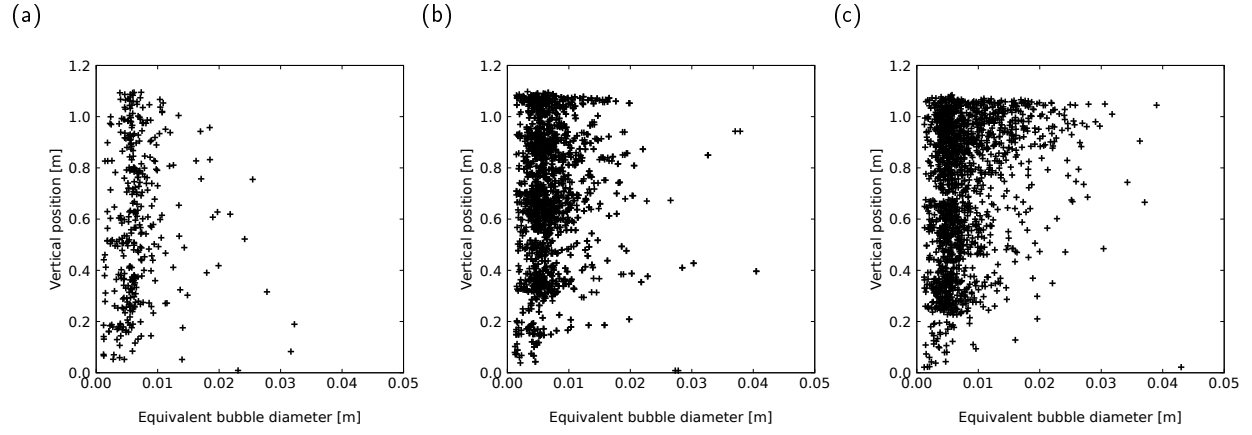

Figure 5: Evolution of equivalent bubble diameter along the pool height ((a) $\dot{Q}$ = 8.5 l/min, (b) $\dot{Q}$ = 42.4 l/min, (c) $\dot{Q}$ = 84.8 l/min)

Further quantitative comparison between the experimental and numerical results is made concerning time-averaged void fraction distributions. As shown in Figure 6 the gas injected from the orifice hole located at $[x, y, z] = [0, 0, 0]$ generates a narrower distribution with higher peaks in the neighbouring region, e.g. at $z = 100\ mm$, and the peak amplitude increases with the gas flow rate. As the gas jet or bubble swarm travels upwards through the pool, the distribution gets rapidly broader while the peak lower because of momentum exchanging with the liquid. In addition, the transverse distribution of void fraction at low heights is found to follow a normal function with the maximum value posited at $x = 0\ m$. With the increasing of travel distance, the location of profile median deviates slightly from the

central line and asymmetrical sides are observed, which is due to unsteady oscillation of the bubble plume and liquid recirculation. According to the simulation results (solid lines), the lower and upper tails of the void fraction distribution become obviously taller close to the free surface, e.g. at $z = 900\ mm$ in the cases of $\dot{Q} = 42.4,\ 84.8\ l/min$. It indicates that the appearance of bubbles beneath the free surface may occur over the whole cross section in addition to the nozzle axis region, which nevetheless agrees with the high-speed camera images taken in the experiment (see Figure 2). The data provided by wire-mesh sensors in cases $\dot{Q} = 8.5,\ 84.8\ l/min$ match the model prediction satisfactorily, as shown in Figures 6(a) and (c), while for the case of $\dot{Q} = 42.4\ l/min$ no data are available in the paper of Abe et al. (2018). The under-estimation of void fraction in the peripheral region at $z = 900\ mm$ by wire-mesh sensor measurements may be attributed to its spatial resolution limit.

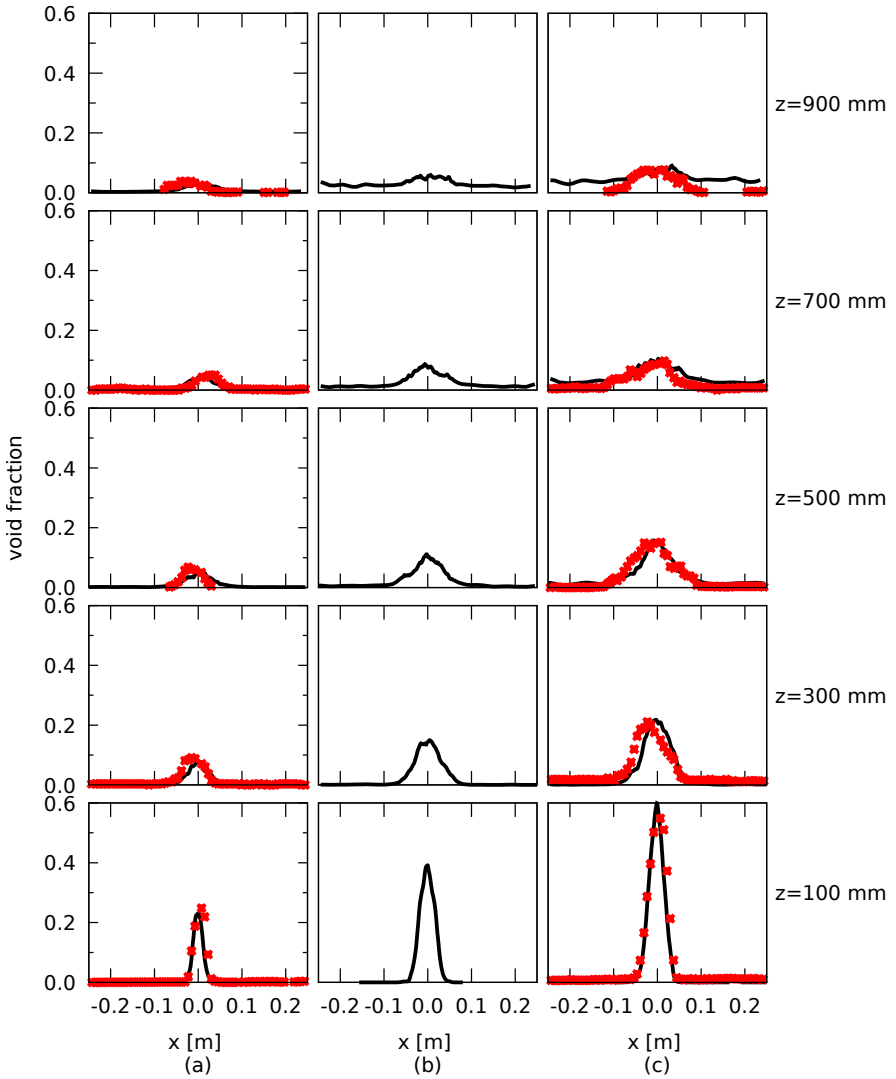

Figure 6: Quantative comparison between measured and simulated transverse void fraction distribution at different height positions ((a) $\dot{Q} = 8.5$ l/min, (b) $\dot{Q} = 42.4$ l/min, (c) $\dot{Q} = 84.8$ l/min, symbol: experiment, line: simulation. The values of z on the right side represent vertical distance of measurement plane away from the nozzle exist, coordinate x refers to the horizontal position relative to the nozzle axis located at x=0 m)

The excellent agreement between the simulated and measured void fraction on the central axis of the gas jet is illustrated further with the help of Figure 7, where the red symbols are experimental data, whereas the lines denote simulation results. The injection of pure gas from the orifice hole on the bottom plate is reflected by $\alpha = 1$ at $z = 0\ m$

, where α and z represents the central void fraction and vertical position of the measurement plane, respectively. As the gas jet travels upwards to the free surface, the void fraction on the central axis decreases rapidly, e.g. below 2.5% at $z = 1.0\ m$ in the case of $\dot{Q} = 8.5\ l/min$. Self-evidently, it will recover to 1 on the free surface as the simulation results show. It should be noted that the sectional averaged void fractions do not vary much in the rise region from $z = 0.3\ m$ to $0.9\ m$, since the volumetric flow rate is given and the mean velocity of gas across the surface remains nearly constant, which will be discussed further below.

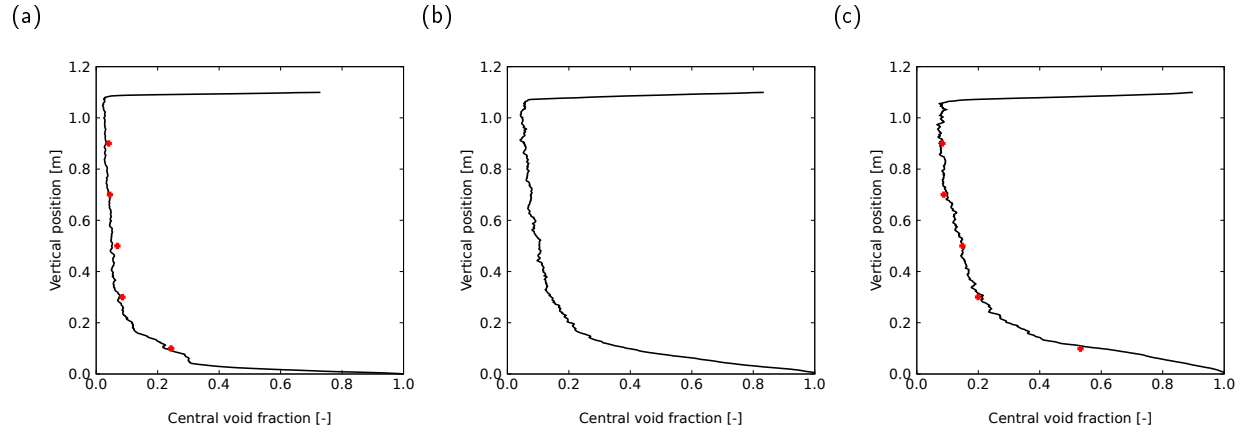

Figure 7: Time-averaged void fraction on the central axis of the nozzle ((a) $\dot{Q} = 8.5$ l/min, (b) $\dot{Q} = 42.4$ l/min, (c) $\dot{Q} = 84.8$ l/min, symbol: experiment, line: simulation)

As aforementioned, in order to explore pool scrubbing dynamics in more detail, bubble tracking techniques are implemented in the simulation. By means of this instanteneous information about the size, shape, position and velocity of all bubbles present in the 3D computational domain is available, which is able to overcome the limitations of optical or wire-mesh measurements to some extent. While the change of bubble size along the pool height is discussed above (see Figure 5), the dependency of bubble velocity on their vertical position is shown in Figure 8. The black crosses are the instantaneous velocities of numerically tracked bubbles in the vertical direction, while the red line in Figures 8 (a) and (c) represents wire-mesh sensor measurements of the gas-phase average velocity that are available in Abe et al. (2018). The interface-capturing results reveal a clear acceleration and/or decceleration zone existing respectively close to the nozzle exit and free surface, which implies strong momentum transfer between the gas jet and surrounding liquid. In the swarm rising zone, say $0.3\ m < z < 0.9\ m$, the average gas or bubble velocity remains almost constant, which is confirmed by both the experiment and simulation. The numerical average velocity is slightly higher than the experimental one at $\dot{Q} = 8.5\ l/min$, while at higher gas injection rates the experiment and simulation results agree well with each other, see Figure 8 (c). Furthermore, it is worth noting that in the experiment the average gas velocity was obtained by using two layers of wire-mesh sensors, whose signals are cross-correlated for each pair of mesh points that are located above each other (Beyer et al., 2008). On the other hand, the numerical results are instantaneous velocities of individual bubble centers. Apart from the effect of spatial positions, the scatter of data is mainly related to a diversity of bubble sizes that are detected as shown in Figure 5. At one vertical position, both the bubble size and velocity are non monotonic. The range of scattering increases with the gas flow rate.

The dependency of bubble rise velocity on its equivalent diameter in the swarm region is analyzed both experimentally and numerically. In Figure 9 black crosses again stand for simulation results, whereas red squares represent the data obtained from either image processing or wire-mesh sensor measurement. The data for small diameter region ($d_b < 3$ mm) were evaluated from visualization images since they tend to go through the wire without measured by WMS, while for $d_b > 3$ mm the two measurements are consistent with each other. It is worth mentioning that the wire-mesh sensor and numerical measurements refer to volumetric diameter of an equivalent sphere, while the image processing method delivers an area equivalent one. Although some lower velocities ($< 0.2\ m/s$) and higher ones for small bubbles ($< 5\ mm$) are detected by the numerical approach compared to the values provided by experiments, a good agreement is evidenced in the case of $\dot{Q} = 8.5\ l/min$. The rising velocity of bubbles increases with the increase

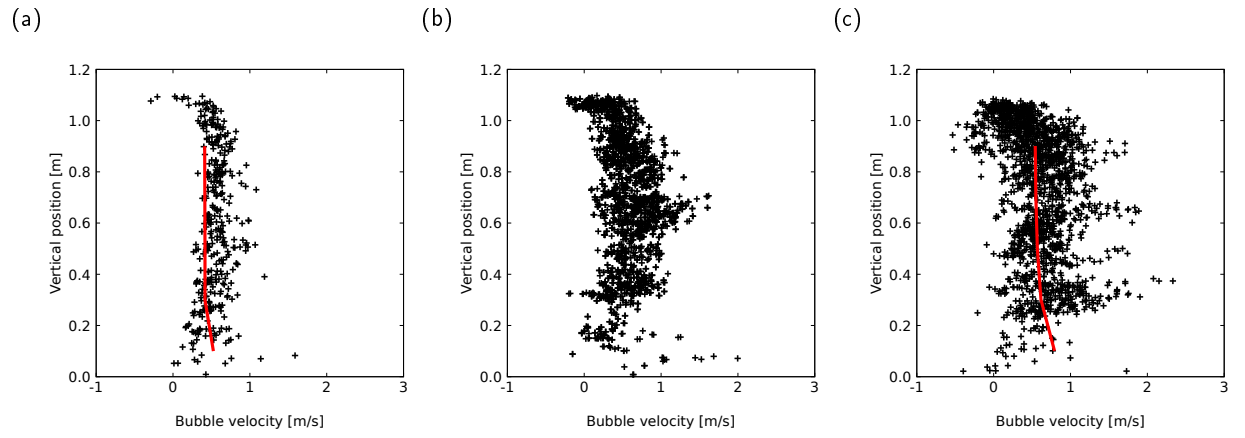

Figure 8: Comparison between velocity of numerically tracked bubbles and average gas velocity measured by wire-mesh sensors ((a) $\dot{Q} = 8.5$ l/min, (b) $\dot{Q} = 42.4$ l/min, (c) $\dot{Q} = 84.8$ l/min, symbol: simulation, line: experiment)

of their sizes due to buoyancy. For example, a bubble having the size over 10 mm may exceed 1.0 m/s during the scrubbing, which is obviously larger than the terminal velocity obtained by using typical correlations for the drag coefficient such as Ishii and Zuber (1979) and Tomiyama et al. (1998). It indicates that swarm effects and drag reduction are significant in the rise region. A similar trend is observed at higher injection rates, where much more large bubbles are formed, which were obviously not all detected and processed in the experiment. The same set of experimental data is plotted in Figures 9(a) $\sim$ (c). Furthermore, the monotonous dependency between the velocity and size is not clear any more, because the number of bubbles as well as the interaction between them increases significantly. The possible range of velocities for a certain bubble size increases as shown in Figures 9 (b) and (c). Furthermore, the maximal rise velocity of bubbles with comparable sizes increases with the injection flow rate. For example in the range of $d = 2 \sim 10$ mm it is almost doubled. The residence time of bubbles inside the pool is naturally a key parameter influencing DF, however, the dependency was found to be nonlinear experimentally by Peyres et al. (1995). On one side the increase of injection velocity tends to reduce the time of bubbles rise through the pool and thus the DF. On the other hand, large breakup rate in the injection zone and centrifugal deposition rate in the rise zone introduced by high velocities increase the DF significantly.

Interfacial area is an important parameter for the evaluation of the scrubbing efficiency under various hydrodynamic conditions. Large interfacial area concentration is beneficial to particle retention. Figure 10 shows the effect of gas flow rate on void fraction, interfacial area concentration and bubble Sauter mean diameter. Since the nozzle diameter is kept constant in this study, gas injection velocity increases with the flow rate, leading to higher void fraction at higher flow rate, and the interfacial area concentration is augmented correspondingly. However, as one can see from Figure 10 (b) the increase is significantly slowed down at high gas flow rates. This is because the interaction and coalescence between bubbles become frequent as the void fraction increases, which produce large bubbles and reduce the interfacial area. The effect of bubble dynamics as well as its dependence on the gas flow rate is elucidated in more detail by the change of the Sauter mean bubble diameter, see Figure 10 (c). At low injection velocities, the mean diameter decreases as a result of bubble breakup, and then increases as the gas flow rate further increases, due to the overtake of coalescence. It evidences that bubble coalescence and breakup events play an important role in the pool scrubbing. As shown in Kim et al. (2021), at a constant flow rate the gas injection velocity decreases rapidly with the increase of nozzle diameter. In other words, the size of injection nozzle is another crucial factor influencing the bubble size, hydrodynamics in the pool and the scrubbing efficiency consequently.

A further advantage of 3D numerical simulations is the capability of providing insights into the whole flow field during pool scrubbing, which is challenging for most experimental techniques at high gas flow rates. The velocity vector fields in the three investigated cases are visualized in Figure 11, where the glyphs are scaled and colored by the velocity magnitude. The grey structures are contour surfaces with $\alpha = 0.5$ indicating the distribution of the gas phase, as shown in Figure 2. The injection of gas gives rise to obvious agitation and displacement of the liquid elements, which

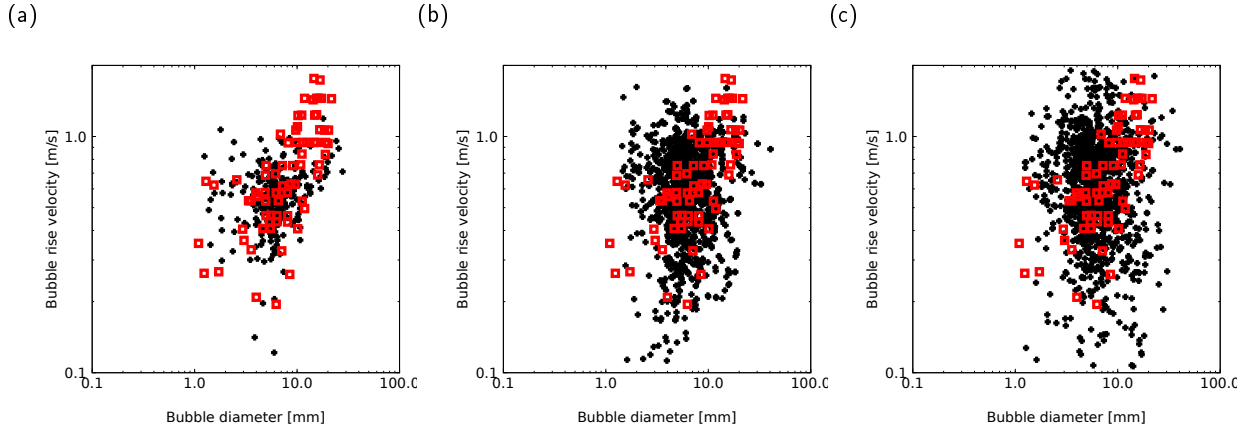

Figure 9: Comparison numerically and experimentally tracked bubble velocities in the rise region ((a) $\dot{Q} = 8.5$ l/min, (b) $\dot{Q} = 42.4$ l/min, (c) $\dot{Q} = 84.8$ l/min, black crosses: simulation, red squares: experiment)

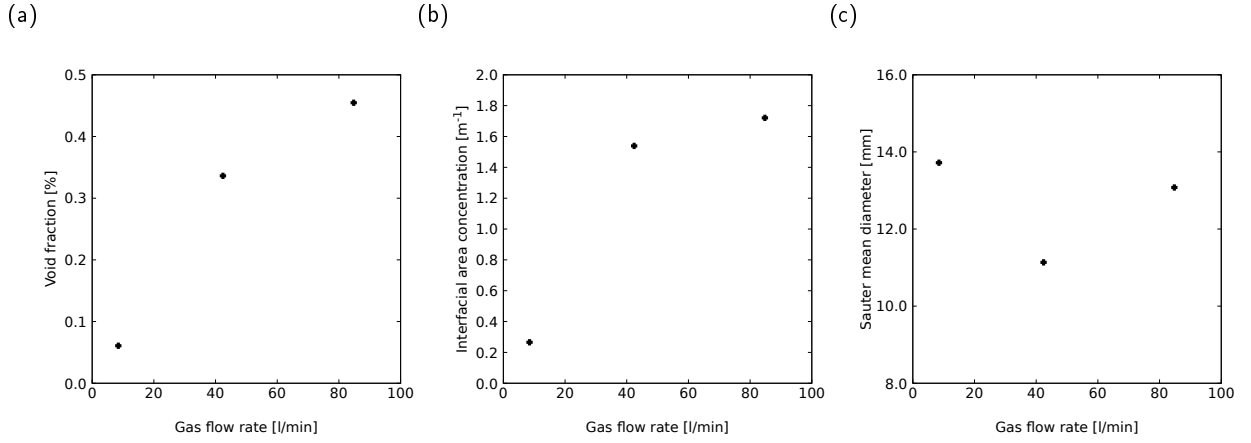

Figure 10: Influence of gas flow rates on (a) void fraction, (b) interfacial area concentration and (c) Sauter mean diameter

are initially stationary. In addition to a major vertical component strong lateral motion is generated at the moment of detachment, which is originated from the globule surface with a magnitude increasing with the gas flow rate. The rapid movement of globules in the injection zone is the major mechanism leading to inertial collision between aerosol particles and bubble-water interface, and contributes to scrubbing efficiency. In the case of $\dot{Q} = 8.5\ l/min$ the motion is confined to the center region, where the gas jet is located. The overall direction of both liquid and gas is upward while no noticeable reverse flow is observed. As the injection rate increases, the whole pool including the proximity of the walls, where no bubbles are present, is agitated, although the major momentum region still coincide with the void fraction distribution. The liquid flows upwards with the rising bubbles from the center up to the free surface and then downwards along the walls. The recirculation orginates from the pool surface due to strong momentum transfer between the gas and the liquid occurring there. The depth towards the bottom and the size of the recirculation zone increases with the injection velocity. The violent interphase interaction both at the point of injection and the free surface promotes the oscillation of the plume formed by the gas jet during its rise. The liquid recirculation and plume oscillation surely have an effect on the residence time and retention efficiency, which should be considered in the determination of the DF.

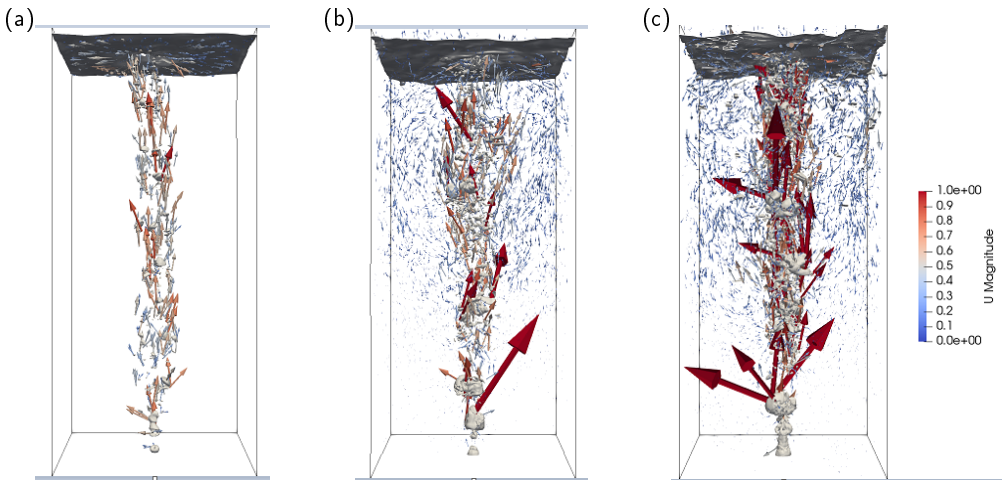

Figure 11: Three-dimensional illustration of the simulated velocity vector field at $t = 20\ s$ ((a) $\dot{Q} = 8.5$ l/min, (b) $\dot{Q} = 42.4$ l/min, (c) $\dot{Q} = 84.8$ l/min)

Finally, in order to evaluate the computational cost of the detailed 3D studies using the VOF interface-tracking method, 15 timesteps as well as the clock time elapsed between two subsequent steps are sampled at the end of simulation, see Table 2. All the simulations were performed on the HPC cluster Hemera at HZDR, and for each simulation one node with 40 cores was used. One can see that for the case $\dot{Q} = 8.5\ l/min$, the mean time step is around $8.33 \times 10^{-5}\ s$. If the function object for tracking bubbles is activiated every 10 timesteps, the completion of 20 s physical time needs 122 $days$. Because the timestep decreases and bubble tracking time increases, the computational cost increases drastically with the gas flow rate. For example, at $\dot{Q} = 84.8\ l/min$, the simulation would finish in 21860 $days$. Since the bubble tracking object is most time-consuming, it was activated only at the end of the simulation in oder to keep a reasonable computational time, which was still over two months in the high-velocity case. Therefore, except the void fraction shown in Figures 6 and 7, the results obtained by the bubble tracking method such as bubble size and rise velocity are not time-averaged but at the time point $t = 20\ s$.

5. Conclusion

Pool scrubbing under globule or jet injection regime is a relevant subject in nuclear safety analysis, since high inlet gas flow rates often expected in severe accident scenarios. The hydrodynamic behavior of globule formation and disintegration as well as rising bubble swarm is a determining factor for particle retention with regards to gas-liquid interfacial area and bubble residence time. Retention of radioactive particles in acqueous pools was intensively investigated in the 80's and a few correlations or modules for pool scrubbing were established at that time, which are encapusalted in some safety analysis codes (He et al., 2021), e.g. ASTEC, MELCOR and COCOSYS . One major weakness of these models is that they have not been validated properly for high gas flow rates (Berna et al., 2016), and have large uncertainties in this regime concerning globuble structure and bubble size/velocity in the swarm region. The objective of the present work is to gain deep insight in the submerged jet under medium and high gas flow rates using a VOF interface-capturing method. Through high-resolution 3D simulations, the gas-liquid interfacial shape as well as its evolution from the orifice to the pool surface is well captured, and the zones of injection, breakup and rise are identified. Besides phase distribution, characteristics of individual bubbles are obtained by additional bubble tracking methods. They are all in a good agreement with laboratory measurements. The detailed information on bubble shape, size and velocity is helpful for understanding the phenomenon of pool retention and validating/developing models for the description of particle removal mechansims. The major findings of the study can be summarized as follows:

- Complex deformation and coalescence behavior is observed during globule formation at the nozzle. The initial size and momentum of globules increases exponentially with the gas flow rate, and significant breakup is detected after the detachment at high flow rates.

	$\dot{Q}$ = 8.5 [l/min]		$\dot{Q}$ = 42.4 [l/min]		$\dot{Q}$ = 84.8 [l/min]	
number	**timestep [s]**	**elapsed time [s]**	**timestep [s]**	**elapsed time [s]**	**timestep [s]**	**elapsed time [s]**
1	8.06×10^{-5}	4	3.62×10^{-5}	24	2.18×10^{-5}	6
2	8.06×10^{-5}	4	3.64×10^{-5}	15	2.17×10^{-5}	6
3	8.13×10^{-5}	3	3.65×10^{-5}	10	2.18×10^{-5}	5
4	8.13×10^{-5}	4	3.64×10^{-5}	9	2.19×10^{-5}	10
5	8.20×10^{-5}	3	3.64×10^{-5}	8	2.21×10^{-5}	11
6	8.35×10^{-5}	13	3.68×10^{-5}	6	2.22×10^{-5}	8
7	8.20×10^{-5}	18	3.68×10^{-5}	6	2.15×10^{-5}	6
8	7.41×10^{-5}	3	3.68×10^{-5}	6	2.06×10^{-5}	6
9	7.41×10^{-5}	9	3.66×10^{-5}	23	2.0×10^{-5}	10
10	7.41×10^{-5}	754*	3.65×10^{-5}	1860*	1.99×10^{-5}	3296*
11	8.22×10^{-5}	10	3.65×10^{-5}	24	1.96×10^{-5}	8
12	8.79×10^{-5}	4	3.64×10^{-5}	12	1.90×10^{-5}	9
13	8.88×10^{-5}	5	3.62×10^{-5}	9	1.86×10^{-5}	8
14	8.97×10^{-5}	6	3.61×10^{-5}	7	1.85×10^{-5}	6
15	9.16×10^{-5}	4	3.59×10^{-5}	6	1.84×10^{-5}	9
16	9.16×10^{-5}	4	3.59×10^{-5}	23	1.84×10^{-5}	7
17	8.18×10^{-5}	4	3.59×10^{-5}	15	1.78×10^{-5}	6
18	8.35×10^{-5}	3	3.59×10^{-5}	25	1.72×10^{-5}	6
19	8.26×10^{-5}	5	3.59×10^{-5}	14	1.68×10^{-5}	6
20	9.19×10^{-5}	731*	3.59×10^{-5}	1889*	1.67×10^{-5}	3348*
mean	8.33×10^{-5}	79.6	3.63×10^{-5}	200	1.97×10^{-5}	339

* Here the function object for tracking bubbles is activated.

Table 2: Overview of automatic time steps and computational speed

- The transition between injection regimes conforms to the Weber number criterion proposed by Yoon and Jeong (2019). Two of the investigated cases belong to the globule regime while the other one having an injection Weber number greater than 10^5, is in the jet regime.
- The size distribution of bubbles generated by the high-speed gas jet fits a log-normal function. The number and maximal size of bubbles increases with the injection velocity, but the mean value is not sensitive. Furthermore, the change of bubble size along the pool height and with the gas flow rate reveals that considerable coalescence takes place at high velocities in the rise region.The slow increase of interfacial area density at the high injection rate indicates that increasing injection rate is not always effective in improving the decontamination factor.
- In the rise region bubble velocity increases with its size. However, the dependency is weaked at high flow rates, where a bubble of a certain size may have a velocity varying from 0.1 to 2.0 m/s. It implies that in addition to buoyancy interfacial stresses play an important role in controlling the bubble movement, and the swarm effect becomes non-negligible.
- The liquid motion induced by bubbles is majorly confined to the centeral region, where the bubbles rise through. With the increase of injection rates, lateral velocity at the surface of detached globules becomes significantly large, which contributes to the scrubbing by enhancing the inertial collision probability between aerosols and bubble surface. Furthermore, liquid recirculation appears at high flow rates, i.e. high upward velocity at the center and downward flow near the walls, which is due to the violent momentum transfer happening between the gas jet and the free surface.

In both injection and rise zones the gas flow rate is shown to have a great influence on the gas-liquid hydrodynamics, and consequently the particle retention in pool scrubbing. The potential contribution of globule disintegration after entering the pool was discussed in Peyres et al. (1995), but the knowledge is still insufficient for considering it in a decontamination factor model. Moreover, the effect of gas entrainment, liquid circulation and bubble swarm occuring

at high injection velocities needs further study. Besides experiments high resolution simulation such as using the VOF method offers a feasible tool for acquiring insights in the complex process, which makes a step towards reliable modelling in system codes.

Acknowledgements

The authors acknowledge Dr. Richard Meller for providing the numerical bubble tracking method. Jiadong Li acknowledges the funding by the Chinese Scholarship Council (CSC).

References

Abe, Y., Fujiwara, K., Saito, S., Yuasa, T., Kaneko, A., 2018. Bubble dynamics with aerosol during pool scrubbing. Nuclear Engineering and Design 337, 96–107.

Albadawi, A., Donoghue, D., Robinson, A., Murray, D., Delauré, Y., 2013. Influence of surface tension implementation in volume of fluid and coupled volume of fluid with level set methods for bubble growth and detachment. International Journal of Multiphase Flow 53, 11–28.

Albiol, T., Herranz, L., Riera, E., Dalibart, C., Lind, T., Del Corno, A., Kärkelä, T., Losch, N., Azambre, B., Mun, C., et al., 2018. Main results of the european passam project on severe accident source term mitigation. Annals of Nuclear Energy 116, 42–56.

Albiol, T., Herranz, L., Riera, E., RSE, A.D.C., Losch, N., Azambre, B., Mun, C., Cantrel, L., 2017. Passive and active systems on severe accident source term mitigation (passam project).

Barron, M.A., Reyes, J., Medina, D.Y., et al., 2020. Bubbling to jetting transition during argon injection in molten steel. World Journal of Engineering and Technology 8, 605.

Berna, C., Escrivá, A., Muñoz-Cobo, J., Herranz, L.E., 2016. Enhancement of the sparc90 code to pool scrubbing events under jet injection regime. Nuclear Engineering and Design 300, 563–577.

Berzal, M.E., Crespo, M.M., Swiderska-Kowalczyk, M., Espigares, M.M., Jimenez, J.L., 1995. State-of-the-art review on fission products aerosol pool scrubbing under severe accident conditions. EUR Report 16241.

Beyer, M., Lucas, D., Kussin, J., Schütz, P., 2008. Air-water experiments in a vertical dn200-pipe .

Boubendir, L., Chikh, S., Tadrist, L., 2020. On the surface tension role in bubble growth and detachment in a micro-tube. International Journal of Multiphase Flow 124, 103196.

Brackbill, J.U., Kothe, D.B., Zemach, C., 1992. A continuum method for modeling surface tension. Journal of computational physics 100, 335–354.

Dehbi, A., Cheng, X., Liao, Y., Okagaki, Y., Pellegrini, M., 2022. A comparative cfd exercise on bubble hydrodynamics using euler-euler and interface tracking approaches, in: The 18th International Topical Meeting on Nuclear Reactor Thermalhydraulics (NURETH-19), Brussel, Belgium, SCK CEN, von Karman Institute for Fluid Dynamics.

Dehbi, A., Suckow, D., Guentay, S., 2001. Aerosol retention in low-subcooling pools under realistic accident conditions. Nuclear Engineering and Design 203, 229–241.

Deshpande, S.S., Anumolu, L., Trujillo, M.F., 2012. Evaluating the performance of the two-phase flow solver interfoam. Computational science & discovery 5, 014016.

Fujiwara, K., Kikuchi, W., Nakamura, Y., Yuasa, T., Saito, S., Kaneko, A., Abe, Y., 2019. Experimental study of single-bubble behavior containing aerosol during pool scrubbing. Nuclear Engineering and Design 348, 159–168.

Georgoulas, A., Koukouvinis, P., Gavaises, M., Marengo, M., 2015. Numerical investigation of quasi-static bubble growth and detachment from submerged orifices in isothermal liquid pools: The effect of varying fluid properties and gravity levels. International Journal of Multiphase Flow 74, 59–78.

Gupta, S., Herranz, L., Van Dorsselaere, J., 2017. Integration of pool scrubbing research to enhance source-term calculations (ipresca), in: The 8th European Review Meeting on Severe Accident Research (ERMSAR2017), Warsaw, Poland.

Hale, J., Akers, C., 2016. Deceleration of droplets that glide along the free surface of a bath. Journal of Fluid Mechanics 803, 313–331.

He, L., Li, Y., Zhou, Y., Chen, S., Tong, L., Cao, X., 2021. Investigation on aerosol pool scrubbing model during severe accidents. Frontiers in Energy Research , 503.

Ishii, M., Zuber, N., 1979. Drag coefficient and relative velocity in bubbly, droplet or particulate flows. AIChE journal 25, 843–855.

Kadoi, K., Nakae, H., 2011. Relationship between foam stabilization and physical properties of particles on aluminum foam production. Materials Transactions , 1108221452–1108221452.

Khan, I., Wang, M., Basit, M.A., Tian, W., Su, G., Qiu, S., 2021. Cfd modeling of liquid entrainment through vertical t-junction of fourth stage automatic depressurization system (ads-4). Annals of Nuclear Energy 159, 108317.

Khan, I., Wang, M., Zhang, Y., Tian, W., Su, G., Qiu, S., 2020. Two-phase bubbly flow simulation using cfd method: A review of models for interfacial forces. Progress in Nuclear Energy 125, 103360.

Kim, Y.H., Yoon, J., Jeong, Y.H., 2021. Experimental study of the nozzle size effect on aerosol removal by pool scrubbing. Nuclear Engineering and Design 385, 111544.

Li, Y., Tong, L., Cao, X., 2021. Experimental study on influencing factors of aerosol retention by pool scrubbing. Frontiers in Energy Research , NA–NA.

Liao, Y., Lucas, D., 2016. Poly-disperse simulation of condensing steam-water flow inside a large vertical pipe. International Journal of Thermal Sciences 104, 194–207.

Liao, Y., Lucas, D., 2020. Simulation of bubble dynamics under pool scrubbing conditions, in: The 8th Computational Fluid Dynamics for Nuclear-Reactor Safety - OECD/NEA workshop (Virtual CFD4NRS-8), Nuclear Energy Agency.

Liao, Y., Lucas, D., Krepper, E., 2014. Application of new closure models for bubble coalescence and breakup to steam–water vertical pipe flow. Nuclear Engineering and Design 279, 126–136.

Ma, J., Li, J., Zhou, P., Song, Y., Chai, L., Zhou, C.Q., 2019. A viewpoint on the dynamics of bubble formation from a submerged nozzle. European Journal of Mechanics-B/Fluids 78, 276–283.

Maiwald, A., Schwarze, R., 2011. Numerical analysis of flow-induced gas entrainment in roll coating. Applied mathematical modelling 35, 3516–3526.

Marchetto, C., Cousin, F., 2019. Proposal of a pool scrubbing modelling for astec: bubble hydrodynamic and thermalhydraulc aspects, in: The 9th European Review Meeting on Severe Accident Research (ERMSAR2019), Clarion Congress Hotel, Prague, Czech Republic.

Marcos, M., Gómez, F., Melches, I., Martín, M., Lopez, M., 1994. Lace-espana experimental programme on the retention of aerosols in water pools. Technical Report CIEMAT-740.

Morandi, S., Corno, A.D., Parozzi, F., Cavallari, A., Besagni, G., Imo, M., Inzoli, F., 2015. Pool scrubbing system for aerosol removal: focus on bubble characteristics and modeling, in: European Aerosol Conference (EAC 2015), ITA.

Nakamura, Y., Fujiwara, K., Kikuchi, W., Yuasa, T., Kaneko, A., Abe, Y., 2019. Experimental study on decontamination effect of gas-liquid two-phase flow behavior with condensation during pool scrubbing, in: The 27th International Conference on Nuclear Engineering (ICONE27), Tsukuba, Ibaraki, Japan, The Japan Society of Mechanical Engineers.

Okagaki, Y., Sibamoto, Y., Abe, S., 2020. Numerical study on bubble hydrodynamics with flow transition for pool scrubbing, in: The 8th Computational Fluid Dynamics for Nuclear-Reactor Safety - OECD/NEA workshop (Virtual CFD4NRS-8), Nuclear Energy Agency.

Ouallal, M., Leyer, S., Gupta, S., 2021. Literature survey of droplet entrainment from water pools. Nuclear Engineering and Design 379, 111188.

Peyres, V., Espigares, M., Polo, J., Escudero, M., Herranz, L., Lopez-Jimenez, J., 1995. Pool scrubbing and hydrodynamic experiments on jet injection regime. Technical Report. Centro de Investigaciones Energeticas.

Pumphrey, H.C., Elmore, P.A., 1990. The entrainment of bubbles by drop impacts. Journal of Fluid Mechanics 220, 539–567.

Quan, S., Hua, J., 2008. Numerical studies of bubble necking in viscous liquids. Physical Review E 77, 066303.

Risso, F., Fabre, J., 1998. Oscillations and breakup of a bubble immersed in a turbulent field. Journal of Fluid Mechanics 372, 323–355.

Srinivasan, V., Salazar, A.J., Saito, K., 2011. Modeling the disintegration of modulated liquid jets using volume-of-fluid (vof) methodology. Applied mathematical modelling 35, 3710–3730.

Tomiyama, A., Kataoka, I., Zun, I., Sakaguchi, T., 1998. Drag coefficients of single bubbles under normal and micro gravity conditions. JSME International Journal Series B Fluids and Thermal Engineering 41, 472–479.

Tran, T., de Maleprade, H., Sun, C., Lohse, D., 2013. Air entrainment during impact of droplets on liquid surfaces. Journal of Fluid Mechanics 726.

Wang, M., Wang, Y., Tian, W., Qiu, S., Su, G., 2021. Recent progress of cfd applications in pwr thermal hydraulics study and future directions. Annals of Nuclear Energy 150, 107836.

Weller, H., 2006. A new approach to vof–based interface capturing methods for incompressible, compressible and cavitating flow.

Yoon, J., Jeong, Y.H., 2019. Observation of air bubble characteristics by a vertical nozzle under pool scrubbing conditions, in: The 18th International Topical Meeting on Nuclear Reactor Thermalhydraulics (NURETH-18), ortland, OR, USA, American Nuclear Society.

Zhang, L., Shoji, M., 2001. Aperiodic bubble formation from a submerged orifice. Chemical Engineering Science 56, 5371–5381.